Visualization of electronic states on atomically smooth graphitic edges with different types of hydrogen termination

Maxim Ziatdinov,[1,*] Shintaro Fujii,[2,†] Koichi Kusakabe,[3] Manabu Kiguchi,[2] Takehiko Mori,[1] and Toshiaki Enoki[2,‡]

[1]*Department of Organic and Polymeric Materials, Tokyo Institute of Technology, 2-12-1, Meguro-ku, Tokyo 152-8552, Japan*

[2]*Department of Chemistry, Tokyo Institute of Technology, 2-12-1, Ookayama, Meguro-ku, Tokyo 152-8551, Japan*

[3]*Graduate School of Engineering Science, Osaka University, 1-3 Machikaneyama-cho, Toyonaka, Osaka 560-8531, Japan*

(Received 27 July 2012; revised manuscript received 21 December 2012; published 20 March 2013)

The relation between electronic structure and hydrogen content at the edges of nanosized holes (nanoholes) in graphite single layer is studied by means of atomically resolved scanning tunneling microscopy and first-principles calculations. Repeatable production of nanoholes with predominantly zigzag hydrogenated edges was realized by bombardment of the top graphene layer of graphite with low-energy (100 eV) Ar^+ ions and its further treatment (etching) in an atomic hydrogen environment. Two main types of nanohole zigzag edge, with a striking contrast to each other, are identified: (i) monohydrogenated zigzag edge supporting edge-localized π state on its boundary; (ii) zigzag edge with repeating two monohydrogenated sites and one dihydrogenated site, without features of the edge-localized state and characterized by a prominent standing wave pattern. Absence of the localized state at a general (chiral) hydrogenated graphitic edge consisting of a mixture of zigzag and armchair fragments is also discussed.

DOI: 10.1103/PhysRevB.87.115427 PACS number(s): 73.22.Pr, 68.37.Ef, 73.20.At

I. INTRODUCTION

Crystalline matter with topologically nontrivial electronic band structure may support a special kind of electronic state on its boundary.[1–4] This is the so-called *edge state* (in two dimensions) or *surface state* (in three dimensions). Graphene is a hexagonal monoatomic sheet of sp^2-bonded carbon atoms in which nontrivial topology arises from the pseudospinorial nature of the π-electron wave function.[5–7] The pseudospin description of the graphene electron wave function plays a crucial role (through a richer set of boundary conditions) in determining electronic structure at the edges of graphene sheets. For instance, it gives rise to a macroscopically degenerated manifold of single particle states (flat band) with nearly zero energy, localized along the *zigzag-shaped* edges of graphene, while such states are absent at the *armchair-shaped* edges.[8–16] The resultant enhancement of the density of states (DOS) occurs at the Fermi level (E_F) of graphene and may give rise to a number of interesting physical phenomena such as specific edge magnetism[17–20] and edge state superconductivity.[21] In addition, with the current trend in nanoscience and nanotechnology it is appealing to tune electronic and magnetic properties of graphene nanostructures via chemical modification of graphene edges. For example, it has been recently shown that structural changes in the carbon backbone at the graphene zigzag edge, such as the presence of defects or self-passivating edge reconstruction, can significantly affect properties of the edge state.[22] In the absence of self-passivating reconstruction edge carbon atoms of any realistic graphene sample are terminated by foreign chemical species. It is surprising, however, that in the great majority of previous experimental reports on graphene edges authors did not focus on the connection between specific foreign chemical species attached to the edge and its electronic (or magnetic) properties.[23]

Here we used a combination of high-resolution ultrahigh vacuum scanning tunneling microscopy (UHV-STM) imaging and density functional theory (DFT) calculations to show that key electronic properties of graphene edges, such as the presence/absence of the edge-localized state on the boundary and electronic wave interference in the edge vicinity, can be in principle controlled by altering the number of hydrogen atoms attached to the edge. Our work provides direct experimental evidence for the coexistence of graphene edges with different types of hydrogen termination.

II. METHODS

A. Experiment

A method of hydrogen etching was employed to fabricate graphene edges contained within nanosized pits (nanoholes) on the surface of highly ordered pyrolytic graphite (HOPG) with Bernal AB stacking. The key point in achieving well-defined structure of graphene edges in nanoholes was to perform all preparation, sample transfer, and measurement procedures strictly under UHV conditions, avoiding contact with ambient environment. First, we introduced nucleation sites for the future formation of nanoholes by covering the surface of HOPG with single atomic vacancies via Ar^+ ion bombardment (ion energy $\approx$ 100 eV, time = 3–4 s) and further annealed at 600 °C to remove all possible contaminations.[24,25] Then, the irradiated graphite surface was exposed to atomic hydrogen. To produce the gas phase of atomic hydrogen, we used a hot tungsten filament, close to the target sample, as a catalyst for thermal dissociation of molecular hydrogen. Compared with previous reports on hydrogen etching of a clean graphite basal plane,[13] the presence of atomic vacancies significantly eased creation of nanoholes, allowing us to use relatively low hydrogen pressure ($\sim 10^{-3}$ Pa), and influenced the final shape of nanohole boundaries—most of the produced nanoholes have predominantly zigzag edges. Because nanoholes are created in a rich atomic/molecular hydrogen environment (in realistic conditions, both atomic and molecular species are present), dangling bonds at the nanoholes' edges are expected to be terminated by hydrogen. Finally, the sample was annealed again at 600 °C for 2 h.

The STM experiments were performed in a constant-current mode. The STM tips were prepared by electrochemical etching of tungsten wire and were further cleaned by Ar^+ ion sputtering (ion energy = 1.0–3.5 keV). It was important to ensure that observed patterns at the graphene edges are not due to the tip artifacts. Thus, only those tips which stably show a clear threefold symmetrical pattern on a clean graphite surface were employed in the experiments. All reported scanning tunneling spectroscopy (STS) curves were obtained using a lock-in technique. The directions of the nanoholes' edges were *unambiguously* determined from a graphite lattice image in the immediate vicinity of the nanohole.

B. Theory

Throughout this paper we treat our etched graphite surface as a "graphene on graphite substrate". While STM is a powerful method to probe surface/edge electronic states, it does not provide enough information by itself regarding true atomic arrangement of carbon and hydrogen atoms at the edges of the nanoholes. Thus, to identify chemical composition of the edges we compared experimental STM results with results obtained from DFT modeling of possible edge structures. The DFT calculations were performed within the local (spin) density approximation [L(S)DA] using the Perdew-Zunger exchange correlation scheme[26] as implemented in the PWSCF code of the QUANTUM ESPRESSO package.[27] Note that accurate DFT modeling of nanoholes whose size is comparable to the experimentally observed structures would require construction of a supercell containing up to several thousand atoms. Needless to say that from the viewpoint of computational costs such calculations are not practicable. We thus computed the properties of hydrogenated graphitic edges using a graphene ribbon model and compared results to the experimentally observed straight edges of sufficient length ($l \geqslant 1$ nm) so that possible effects due to the presence of the nanoholes' corner sites can be neglected. To avoid intraedge interactions the ribbons of sufficiently large width ($W = 3.25$ nm) were chosen. For the ultrasoft pseudopotentials (US-PP)[28] adopted here, the cutoff energy for the expansion of wave functions was set to 25 Ry to calculate the optimized geometries. All atoms were fully relaxed until the forces were less than 10^{-3} Ry/a.u. For simulations of STM images the wave function cutoff energy was set to 60 Ry. The Brillouin zone integration was performed using a uniform $8 \times 8 \times 1$ Monkhorst-type k-point grid.[29] The all-electron projector augmented wave (PAW) potentials[30] were also adopted to confirm convergence in magnetic solutions to the STS observation. An effect of the graphite substrate was taken into account by inclusion of the second ("bulk") graphene layer in our slab model. Experimental and simulated data were compared within the Tersoff-Hamann approximation.[31,32] In this approach the low-bias STM images obtained at constant tunneling current represent contour maps of constant surface local density of states (LDOS) at E_F.

III. RESULTS AND DISCUSSION

The topographic STM image of one of the nanoholes prepared by the above-described method is shown in Fig. 1.

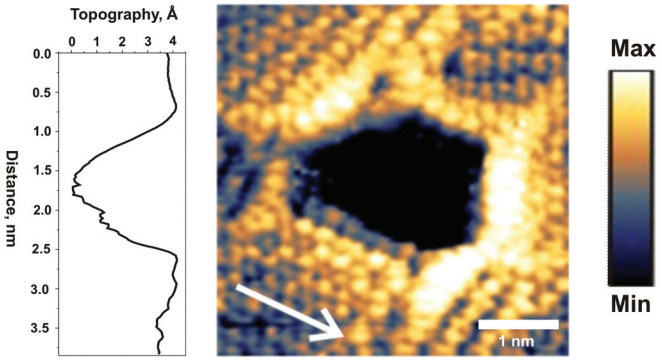

FIG. 1. (Color) Experimental STM image of one of the nanoholes prepared by atomic hydrogen etching. (Imaging conditions: $U = 0.1$ V, $I = 0.9$ nA). Arrow indicates the zigzag direction of graphene lattice. The edges of the nanohole whose directions are related to the direction of the arrow by 0°, 60°, or 120° are zigzag edges. One can see that the depicted nanohole contains mostly zigzag edges. Vertical line scan across the nanohole is shown to the left of the image.

In order to have reliable data on the electronic structure of hydrogenated graphene edges in nanoholes we obtained a sufficiently large number of atomically resolved STM images of nanoholes of different sizes and geometries. All observed nanoholes were only one graphene layer in thickness. Two main types of nanohole edges propagating in the zigzag direction of graphene lattice were identified (see Sec. A in Supplemental Material[33] for determination of edge directions on graphite lattice): (1) zigzag edge with amplitude maximum of the edge-localized state at the outer edge carbon atoms; (2) zigzag edge without features of the localized state, with well-defined superperiodic pattern (superlattice) extended over 1.5–3 nm away from the edge. Below we provide an in-depth description of each type of the observed zigzag edges.

The type 1 zigzag edge is characterized by significant enhancement of topographic contrast (bright spots on STM image) along the edge boundary [Fig. 2(a)]. The average distance between topographic maxima along the edge direction is 0.25 nm, close to the graphene lattice constant (0.246 nm). This indicates the presence of a localized state at each hydrogenated edge carbon atom. For the given periodicity, we need to consider two possible structures: monohydrogenated zigzag edge [Z(1) edge] and dihydrogenated zigzag edge [Z(2) edge]. To distinguish between the Z(1) and Z(2) edge structures experimentally we closely examined a spatial distribution of charge density in the localized state on the boundary of the nanohole. In the low-bias experimental STM image we observe a nearly ellipsoidal distribution of charge density in the localized state "stretched" in the direction *perpendicular* to the edge [Fig. 2(a)]. This is in good agreement with DFT STM simulations for both graphene ribbons and nanoholes with monohydrogenated zigzag edges [Fig. 2(b)]. On the other hand, for a purely dihydrogenated zigzag boundary, maximum elongation in distribution of the edge state charge density is expected in the direction *parallel* to the edge (Sec. B in the Supplemental Material[33]). This has not been observed experimentally. We therefore conclude that the type 1 zigzag edge is a realization of the monohydrogenated zigzag, Z(1), edge.[34] The analysis of the thermodynamic stability of

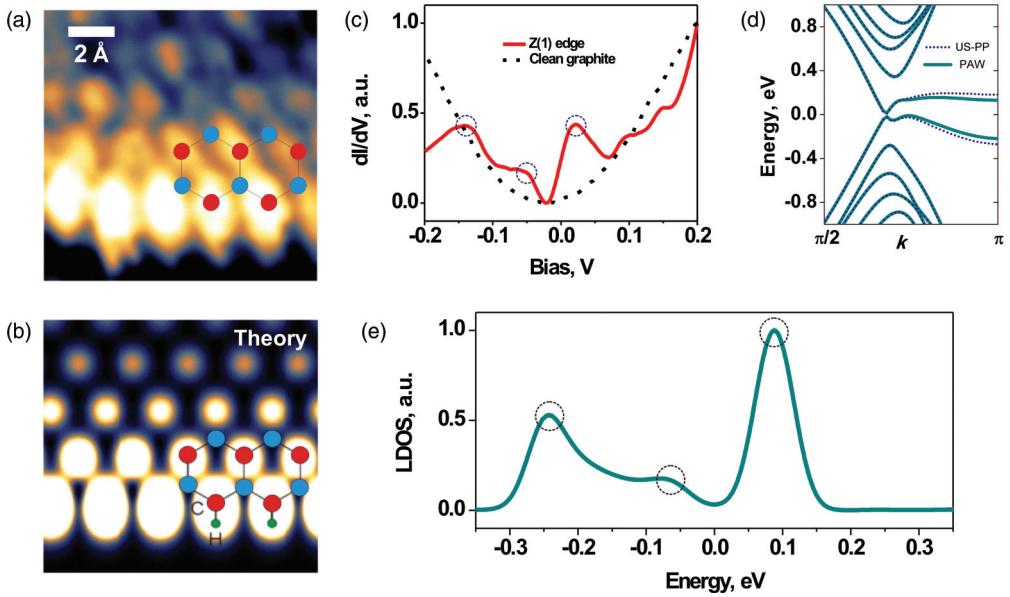

FIG. 2. (Color) (a) Experimental STM image of type 1 zigzag edge, Z(1) ($U = 0.1$ V, $I = 0.7$ nA) and (b) DFT STM simulation at bias voltage $U = 0.1$ V for monohydrogenated zigzag edge. The graphene lattice is shown schematically in (a) and (b) and the hydrogen atoms at the edge are also shown in (b). (c) Normalized averaged dI/dV curve acquired at the Z(1) edge. A tunneling spectrum taken on the clean graphite surface is shown for reference. (d) DFT LSDA band structure for Z(1) graphene ribbon with inclusion of graphite substrate effect calculated with ultrasoft pseudopotentials (US-PP) and projector augmented wave (PAW) potentials (see text). Note that dispersion character of the spin-split edge state bands depends on the choice of the potentials (PAW or US-PP), while bulk band structure is identical for both methods. (e) Theoretical LDOS on the outer edge carbon atom of the Z(1) edge. The LDOS was calculated with the PAW potentials. The dashed circles in (c) and (e) are guides for the eye.

graphene edges which was done by plotting the free energy of edges formation versus the chemical potential of atomic and molecular hydrogen (Sec. C in the Supplemental Material[33]) suggests that for current preparation conditions (temperature, pressure) formation of the Z(1) edge is favored in the presence of molecular hydrogen species. It is noteworthy that in the absence of atomic vacancies, creation of nanoholes would require a significantly larger hydrogen pressure at which the Z(1) edge may not be stable.[35]

STS measurements (that is, dI/dV versus V measurements) at the Z(1) edge reveal a presence of two peaks in the positive and negative bias regions, and a shoulder feature between them [Fig. 2(c)]. The interpeak separation distance is about 0.16 V. These observations are in good *qualitative* agreement with previously reported LSDA calculations on monohydrogenated graphene zigzag ribbon where the presence of two peaks in the LDOS above and below E_F originates from the Stoner spin-splitting of the edge state.[36] On the other hand, there is an apparent discrepancy between the theoretically predicted size of the "magnetic gap" for monolayer graphene (0.5 eV)[36] and the experimentally observed one (0.16 eV). As it follows from our LSDA DFT analysis [Figs. 2(d) and 2(e)], the gap is reduced by nearly 0.1 eV after adding the second (bulk) graphene layer while addition of the next layers (i.e., third-, fourth-bulk layers) almost does not change the size of the gap. Interestingly, by replacing US pseudopotentials with PAW potentials (kinetic energy cutoff set to 40 Ry) we found, for the same Z(1) ribbon structure independently on the number of underlying graphite substrate layers, reduction in the gap size by around 0.1 eV [see Sec. D in the Supplemental Material[33] for details].

The remaining discrepancy between theoretical LDOS at the edge atom of the Z(1) edge [Fig. 2(e)] and experimental STS data [Fig. 2(c)] may be explained by taking into account possible dependence of the magnetic gap structure on the relative position of the edges-containing graphene top layer with respect to the underlying graphite substrate layer(s). Indeed, it has been recently shown, within LSDA, that reduction of the interlayer distance by 0.07 nm reduces the size of the magnetic gap in bilayer graphene nanoribbons by a factor of 4.[37] We found the similar trend in our theoretical model (graphene ribbon on bulk graphite). However, the experimental value of separation between top (edges-containing) layer and underlying (substrate) layer, extracted from STM topography, is nearly equal to the equilibrium interlayer spacing in graphite ($\approx$0.335 nm). Therefore, the argument of reduced interlayer separation seems to be not valid for our sample. On the other hand, careful comparison of experimental STM topographic and theoretical STM electronic density (STM-ED) distance dependence at the Z(1) edge (Fig. 3) shows that the experimental peak height at the edge boundary is much smaller than one can expect from the theory. We recall that the resultant STM topographic signal represents here a sum of possible height variations at the edge (e.g., edge curvature) and edge state related high electronic local density of states. This may suggest that the observed drop in the experimental peak height is related to edge bending towards the underlying (substrate) layer. We found from LSDA

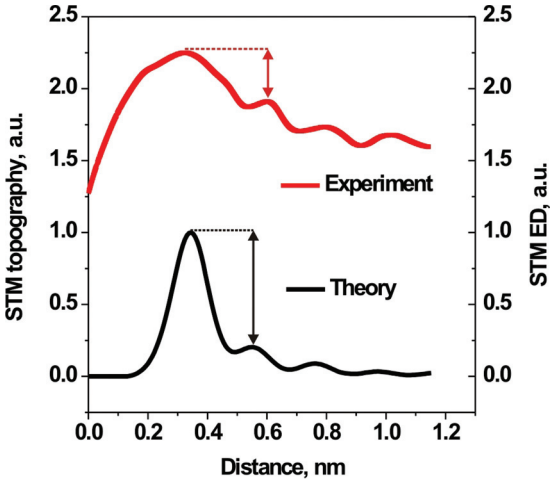

FIG. 3. (Color) Comparison of averaged (over the whole width of the edge) STM topographic profile in the direction perpendicular to the edge in Fig. 2(a) and corresponding theoretical STM electronic density (STM ED) profile. Both curves are normalized so that the signal from the edge boundary corresponds to 1 while the signal from the second layer corresponds to 0. The experimental STM topographic profile is shifted up for clarity. The arrows schematically show the difference between experiment and theory on the relative heights of the first and second peaks. Since the calculations were performed on the (quasi-) flat model the discrepancy may suggest the presence of the edge curvature effects. Such discrepancy was detected at nearly all observed Z(1) edges, although the exact form of decay of the STM topographic signal depends on the type of the edge sublattice termination (A or B) and surface morphology (e.g., density of nanoholes on the surface).

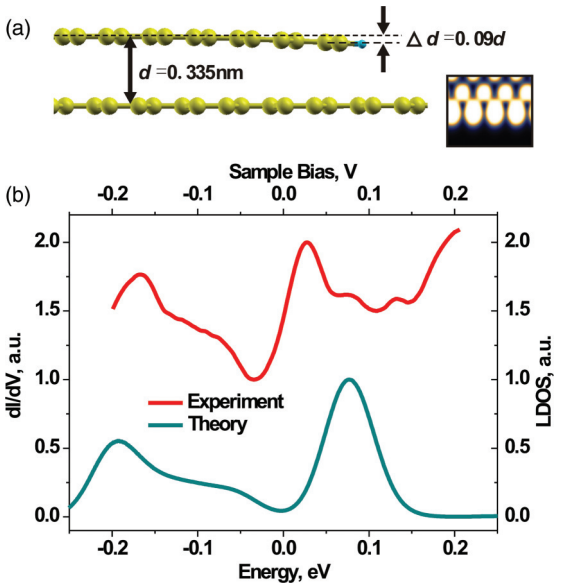

FIG. 4. (Color) (a) Local edge bending effect for the Z(1) edge. The edge atom is shifted towards the second layer by approximately 0.03 nm. The atomic positions in the top and bottom layers were independently fully relaxed and the interlayer distance was adjusted to the equilibrium graphite interlayer distance. The energy cost of the edge bending in the top layer is ≈0.6 meV. The inset in (a) shows no significant changes in charge-density spatial distribution compared to the (quasi-) flat case in Fig. 2(b). (b) Comparison of one of the experimental single STS spectra at the Z(1) edge and theoretical LDOS data, calculated using PAW potentials, for a monohydrogenated edge carbon atom in (a). The experimental STS curve is shifted up for clarity.

that such local edge bending can lead to the reduction of the magnetic gap in our model, similar to the case of the decreased interlayer distance between two "flat" layers. In Fig. 4 we demonstrate an example of such edge bending effect. Although both the flat model in Fig. 2(b) and the model with local edge bending in Fig. 4(a) show almost the same spatial character of the edge state charge-density distribution (in good agreement with experimental STM images), the latter provides considerably better agreement with experimental STS data, as we demonstrate in Fig. 4(b).

The STM image (raw data) of the second type of the zigzag edge is shown in Fig. 5(a). No signatures of the edge-localized π state are revealed for this edge (including dI/dV data). Furthermore, it is characterized by $\sqrt{3} \times \sqrt{3}R30^\circ$ modulation of LDOS in a form of honeycomb superlattice—a feature previously observed only in the presence of armchair edge and explained by the intervalley scattering of extended π-electronic states.[15,38–41] To reproduce these two main features we must go beyond the simple model of the defect-free zigzag edge in which every edge carbon site is terminated by a single hydrogen atom. Our DFT analysis shows (Sec. E in the Supplemental Material[33]) that the edge state (flat band at zero energy) can be removed from the graphene zigzag edge when every third edge site represents the so-called Klein site,[42] either due to dihydrogenation[35] [Z(211) edge] or addition of the sp^2-bonded carbon atom (terminated with two hydrogen atoms, i.e., CH_2 functional group) [Z(C211) edge]. In both cases, the modified zigzag edge can be represented by the Kekule structure(s). Remarkably, for the double-layer graphene model employed here, the DFT STM simulations for both Z(211) and Z(C211) edges show nearly identical charge-density patterns, which are also in very good agreement with the experimental STM image. We note, however, that dangling carbon sites are usually attached to the zigzag boundaries of nanoholes in a random manner, as was observed in current experiments. This suggests that one cannot expect a realization of long-range periodic edge structure containing CH_2 functional groups. On the other hand, our analysis of thermodynamical stability indicates that long-range periodic edge structure with every third site being dihydrogenated can be formed in an atomic hydrogen environment in current preparation conditions (see Sec. C in the Supplemental Material[33]). Thus, for sufficiently long nanohole edges ($l \geqslant 6a_0$, where a_0 is graphene lattice constant) we recognize the experimentally observed type 2 zigzag edge as a realization of the Z(211) edge. (Note that zigzag edge structures lacking every third edge carbon atom also do not support edge state; however, observation of a well-defined signal from the Klein site in the experimental images of the type 2 zigzag edge, as shown in Sec. F in the Supplemental Material,[33] rules out this explanation). The Z(211) type of edge has been recently theoretically proposed by Wassmann *et al.*[35] as the most stable zigzag edge structure at "conventional" hydrogen pressure. For our preparation conditions, we estimated frequency P of appearance of the Z(1) and (Z211) edges in the STM experiment as $P_{Z(1)}/P_{Z(211)} \geqslant 10$,

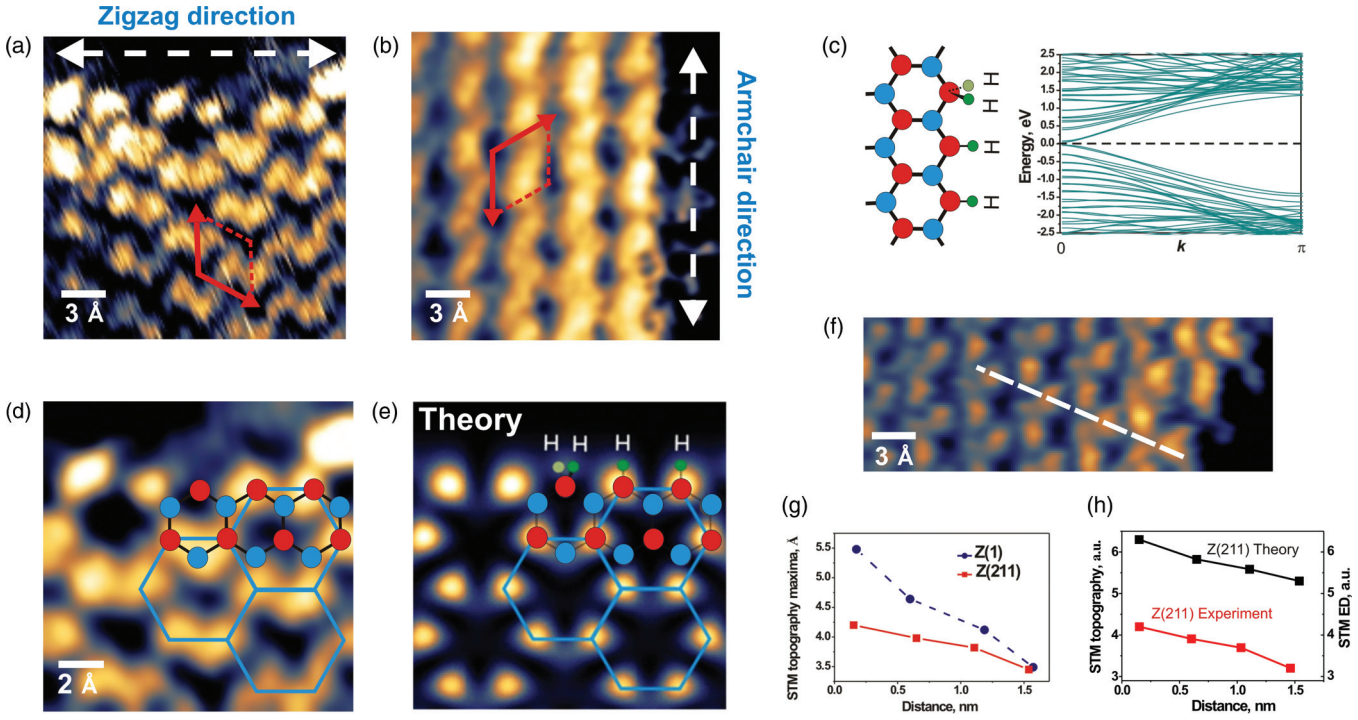

FIG. 5. (Color) Experimental STM image of (a) type 2 zigzag edge, Z(211) ($U = 0.1$ V, $I = 0.7$ nA), and (b) monohydrogenated armchair edge for comparison ($U = 0.3$ V, $I = 0.1$ nA). No image processing, except for rotation, has been applied to the data in (a). The white arrow shows direction of the edge, while the red arrow indicates direction of the superlattice translational vector. The length of the superlattice vector is $\sqrt{3}a_0$, where a_0 is the graphene lattice vector. For the case of the Z(211) edge the superlattice vector is related to the edge direction by 90° (30°), while for the armchair edge the angle is 0° (60°). (c) Electronic band structure calculated for the Z(211) ribbon (with underlying bulk layer) showing no signature of the edge state. (d) Experimental (smoothed) STM image of the Z(211) edge. (e) DFT STM simulations at $U = 0.1$ V for the Z(211) edge. The simulations were performed for a case when zigzag edge is terminated with B-sublattice atoms (no underlying substrate atoms). The honeycomb superlattice is depicted with blue hexagons, and the graphene lattice is shown in both (d) and (e). The positions of mono- and dihydrogenated edge sites are also shown in (e). (f) Fragment of the Z(211) edge from separate experiment with different STM tip compared to (a) and (d). ($U = 0.05$ V, $I = 0.7$ nA). (g) Experimental topographic maxima distribution along dashed white line in (f); corresponding distribution for the Z(1) edge at the same imaging conditions is given for comparison. Satellite signals from minor sublattice have been filtered out in both cases. The difference between topographic height, Δh, on the boundary of the Z(1) and Z(211) edges, is typically $\Delta h = h_{Z(1)} - h_{Z(211)} \approx 1.25$ Å. (h) Comparison of normalized experimental topographic maxima distribution in (g) and calculated STM ED maxima distribution along the same direction. The experimental and theoretical profiles are shifted apart from each other for clarity.

which can be explained as due to the considerably smaller mole fraction of atomic hydrogen in the preparation chamber.[43]

The honeycomb superlattice at the Z(211) edge boundary in Fig. 5(a) can be reproduced after inclusion of the second (bulk) graphene layer in the STM simulation. This allows us to take into account the effect of the graphite substrate on the sublattice selectivity in the STM image. For single-layer graphene, the charge-density pattern at the Z(211) edge boundary represents a continuous "wavelike" structure, similar to that of pure armchair edge in monolayer graphene.[39] It is easy to show within DFT STM simulations that this pattern is not symmetric with respect to the change of the sublattice in a case of AB-stacked graphene sheets. We found that a honeycomb superlattice appears in a computed STM image when the Z(211) edge is terminated with B-sublattice atoms (no underlying graphite substrate atoms) showing nearly perfect matching with the experimental data [Figs. 5(d) and 5(e)]. Thus, in graphene systems with two or more layers honeycomb superlattice does not necessarily occur only in the presence of the armchair-shaped edge, as was assumed previously, but can be also observed at a pure zigzag-shaped edge if a certain type of hydrogen termination is realized at the edge. Compared to the Z(1) edge, we did not find any significant differences between experimental STM topography and theoretical STM ED data at the Z(211) edge [Fig. 5(h)]. This suggests that local edge bending proposed previously may be sensitive to the particular chemical environment at the edge boundary, although a better understanding of the edge formation process in current preparation conditions is required. Note that in the absence of atomically resolved data on the graphene edge one can in principle distinguish between the Z(211) edge and the (mono-/di-) hydrogenated armchair edge by measuring the angle between the superlattice "direction" and the direction of the edge boundary, as illustrated in Figs. 5(a) and 5(b). Structural imperfections along the Z(211) edge can cause interrupted periodicity of the superlattice.

We now turn to the description of the electronic states at the general (chiral) graphene edge, i.e., the edge containing both zigzag and armchair fragments. Such chiral edges are expected to support the edge-localized state at their zigzag fragments.[12,16] In Fig. 6(a), we show a simultaneous imaging of the Z(1) and (4,1) chiral edges, separated by an armchair edge.

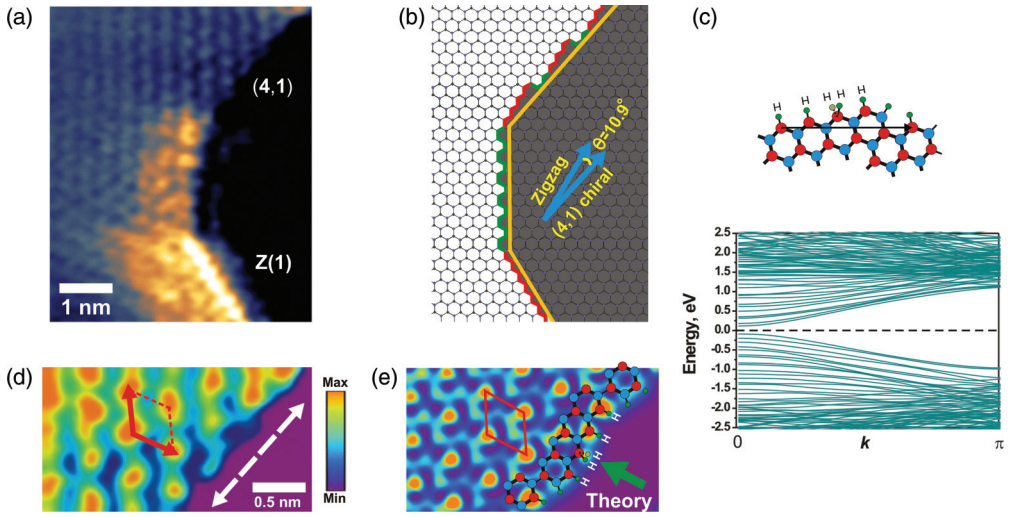

FIG. 6. (Color) (a) Simultaneous experimental observation of the Z(1) and (4,1) edges within one nanohole. ($U = 0.3$ V, $I = 0.35$ nA). (b) Directions of edges in (a) are mapped onto the honeycomb lattice for clarity. (c). Electronic band structure calculation for (4,1) ribbon (including underlying bulk layer) with dihydrogenated site at the zigzag fragment and without signature of the edge state. The translational vector of the (4,1) ribbon is shown by black arrow. (d) Experimentally observed rhombic superlattice at the (4,1) edge in (a). The different contrast is chosen for better visualization. The superlattice vector is denoted by red arrows. Direction of the edge, determined from (a), is denoted by white dashed arrow. (e) DFT STM simulations ($U = 0.3$ V) reproduces rhombic superlattice (companioned with the absence of the edge state) at the (4,1) edge when it is terminated with A-sublattice atoms (with underlying substrate atoms) and dihydrogenated site, denoted by green arrow, is adjusted to armchair fragment of the edge.

Contrary to previous reports on chiral edges, the observed (4,1) edge does not show any features of enhanced LDOS related to the presence of the edge state and is characterized by $\sqrt{3} \times \sqrt{3}R30^\circ$ rhombic superlattice extended over several nanometers away from the edge. In line with discussion for the Z(211) edge we found from DFT that the edge state can be eliminated from the (4,1) edge by saturating one of the sites at its zigzag fragment with two hydrogen atoms [Fig. 6(c)]. Then, each zigzag fragment of the (4,1) edge can be thought of as a realization of a single unit cell of the Z(211) edge. The exact form of superperiodic pattern at the (4,1) edge with the dihydrogenated site is sensitive to the relative position of the dihydrogenated carbon atom with respect to the armchair fragment, as well as to the sublattice termination. The best match with the experimental data was found for the A-sublattice edge (with underlying graphite substrate atoms) where dihydrogenation occurs at the zigzag site adjusted to the armchair fragment, as shown in Figs. 6(d) and 6(e). We note in passing that the armchair edge in Fig. 6(a) does show evidence for the enhanced LDOS at its boundary. The appearance of the localized state at the armchair boundary can occur due to *partial* dihydrogenation of the armchair sites.

IV. CONCLUSIONS

Our findings mark an important step towards bringing together chemical and physical aspects of graphene edges and may have strong implications for the research field of graphene-based nanoscale systems. It has been generally accepted that while the zigzag edge of graphene supports the localized π state on its boundary and gives rise to *intravalley* scattering of extended electronic states, its armchair counterpart does not possess the edge state and leads to *intervalley* scattering of charge carriers.[8–16,38–41] The findings presented here provide experimental evidence that these key distinctions between zigzag and armchair edges of graphene can be completely eliminated by proper attachment of foreign chemical species (namely, hydrogen) to the zigzag edge. This may open a way for tuning electronic and magnetic properties of graphene-based nanostructures (such as graphene nanoribbons, dots, and antidotes) not only by changing the geometrical shape of graphene edges but also by controlling how specific chemical species are attached to the graphene edge of a given geometry. Our results are not restricted to only high-symmetric directions of graphene edges, since we have also shown a possibility of the absence of the localized state at the general edge containing a mixture of zigzag and armchair fragments.

Note added. Very recently we became aware of the similar studies by Zhang *et al.*[44] and Talirz *et al.*[45]

ACKNOWLEDGMENTS

This work was supported by Grant-in-Aid for Scientific Research (Grants No. 20001006 and No. 23750150) from MEXT, Japan. The authors thank the Supercomputer Center, Institute for Solid State Physics, University of Tokyo for the use of the facilities.

*ziatdinov.m.aa@m.titech.ac.jp
†fujii.s.af@m.titech.ac.jp
‡enoki.t.aa@m.titech.ac.jp

[1] D. J. Thouless, M. Kohmoto, M. P. Nightingale, and M. den Nijs, Phys. Rev. Lett. **49**, 405 (1982).
[2] Y. Hatsugai, Phys. Rev. Lett. **71**, 3697 (1993).

[3]S. Ryu and Y. Hatsugai, Phys. Rev. Lett. **89**, 077002 (2002).
[4]C. L. Kane and E. J. Mele, Phys. Rev. Lett. **95**, 146802 (2005).
[5]A. K. Geim and K. S. Novoselov, Nat. Mater. **6**, 183 (2007).
[6]A. H. Castro Neto, F. Guinea, N. M. R. Peres, K. S. Novoselov, and A. K. Geim, Rev. Mod. Phys. **81**, 109 (2009).
[7]D. S. L. Abergel, V. Apalkov, J. Berashevich, K. Ziegler, and T. Chakraborty, Adv. Phys. **59**, 261 (2010).
[8]M. Fujita, K. Wakabayashi, K. Nakada, and K. Kusakabe, J. Phys. Soc. Jpn. **65**, 1920 (1996).
[9]K. Nakada, M. Fujita, G. Dresselhaus, and M. S. Dresselhaus, Phys. Rev. B **54**, 17954 (1996).
[10]L. Brey and H. A. Fertig, Phys. Rev. B **73**, 235411 (2006).
[11]K. Sasaki and R. Saito, Prog. Theor. Phys. Suppl. **176**, 253 (2008).
[12]A. R. Akhmerov and C. W. J. Beenakker, Phys. Rev. B **77**, 085423 (2008).
[13]Z. Kluzek, Z. Wapar, E. A. Denisov, T. N. Kompaniets, I. V. Makarenko, A. N. Titkov, and A. S. Bhatti, Appl. Surf. Sci. **161**, 508 (2000).
[14]Y. Kobayashi, K. Fukui, T. Enoki, and K. Kusakabe, Phys. Rev. B **73**, 125415 (2006).
[15]Y. Niimi, T. Matsui, H. Kambara, K. Tagami, M. Tsukada, and H. Fukuyama, Phys. Rev. B **73**, 085421 (2006).
[16]C. Tao, L. Jiao, O. V. Yazyev, Y.-C. Chen, J. Feng, X. Zhang, R. B. Capaz, J. M. Tour, A. Zettl, S. G. Louie, H. Dai, and M. F. Crommie, Nat. Phys. **7**, 616 (2011).
[17]Y.-W. Son, M. L. Cohen, and S. G. Louie, Nature **444**, 347 (2006).
[18]O. V. Yazyev and M. I. Katsnelson, Phys. Rev. Lett. **100**, 047209 (2008).
[19]K. Kusakabe and M. Maruyama, Phys. Rev. B **67**, 092406 (2003).
[20]H. Lee, Y.-W. Son, N. Park, S. Han, and J. Yu, Phys. Rev. B **72**, 174431 (2005).
[21]K. Sasaki, J. Jiang, R. Saito, S. Onari, and Y. Tanaka, J. Phys. Soc. Jpn. **76**, 033702 (2007).
[22]M. Pan, E. C. Girao, X. Jia, S. Bhaviripudi, Q. Li, J. Kong, V. Meunier, and M. S. Dresselhaus, Nano Lett. **12**, 1928 (2012).
[23]For a review of recent progress in graphene edges characterization, see X. Jia, J. Campos-Delgado, M. Terrones, V. Meunier, and M. S. Dresselhaus, Nanoscale **3**, 86 (2011).
[24]J. R. Hahn and H. Kang, Phys. Rev. B **60**, 6007 (1999).
[25]W. Choi, C. Kim, and H. Kang, Surf. Sci. **281**, 323 (1993).
[26]J. P. Perdew and A. Zunger, Phys. Rev. B **23**, 5048 (1981).
[27]P. Giannozzi *et al*., J. Phys.: Condens. Matter **21**, 395502 (2009).
[28]D. Vanderbilt, Phys. Rev. B **41**, 7892 (1990).
[29]H. J. Monkhorst and J. D. Pack, Phys. Rev. B **13**, 5188 (1976).
[30]P. E. Blochl, Phys Rev B **50**, 17953 (1994).
[31]J. Tersoff and D. R. Hamann, Phys. Rev. Lett. **50**, 1998 (1983).
[32]J. Tersoff and D. R. Hamann, Phys. Rev. B **31**, 805 (1985).
[33]See Supplemental Material at http://link.aps.org/supplemental/10.1103/PhysRevB.87.115427 for determination of edge directions, analysis of thermodynamic stability of the observed edges, DFT STM simulations for the Z(2) and Z(C211) edges, tests for adopted PAW potentials and US-PP, and identification of the STM signal from dihydrogen complex at the Z(211) edge.
[34]The inclusion (exclusion) of spin component in LDA (from LSDA) DFT STM simulations does not change the character of the edge state charge distribution at the boundary of the Z(1) and Z(2) edges.
[35]T. Wassmann, A. P. Seitsonen, A. M. Saitta, M. Lazzeri, and F. Mauri, Phys. Rev. Lett. **101**, 096402 (2008).
[36]J. Jiang, W. Lu, and J. Bernholc, Phys. Rev. Lett. **101**, 246803 (2008).
[37]Y. Guo, W. Guo, and C. Chen, J. Phys. Chem. C **114**, 13098 (2010).
[38]K. Sakai, K. Takai, K. Fukui, T. Nakanishi, and T. Enoki, Phys. Rev. B **81**, 235417 (2010).
[39]K. Sasaki, K. Wakabayashi, and T. Enoki, J. Phys. Soc. Jpn. **80**, 044710 (2011).
[40]C. Park, H. Yang, A. J. Mayne, G. Dujardin, S. Seo, and Y. Kuk, Proc. Natl. Acad. Sci. USA **108**, 18622 (2011).
[41]J. Tian, H. Cao, W. Wu, Q. Yu, and Y. P. Chen, Nano Lett. **11**, 3663 (2011).
[42]D. J. Klein, Chem. Phys. Lett. **217**, 261 (1994).
[43]X. Qi, Z. Chen, and G. Wang, J. Mater. Sci. Technol. **19**, 235 (2003).
[44]X. Zhang, O. V. Yazyev, J. Feng, L. Xie, C. Tao, Y. Chen, L. Jiao, Z. Pedramrazi, A. Zettl, S. G. Louie, H. Dai, and M. F. Crommie, ACS Nano **7**, 198 (2013).
[45]L. Talirz, H. Söde, J. Cai, P. Ruffieux, S. Blankenburg, R. Jafaar, R. Berger, X. Feng, K. Müllen, D. Passerone, R. Fasel, and C. A. Pignedoli, J. Am. Chem. Soc. **135**, 2060 (2013).